

# The Evolution of Galaxies in and around Clusters at High-Redshift

Yutaka FUJITA

*National Astronomical Observatory,*

*and*

*Department of Astronomical Science, The Graduate University for Advanced Studies,*

*2-21-1 Osawa, Mitaka, Tokyo 181-8588*

*yfujita@th.nao.ac.jp*

*and*

Tomotsugu GOTO

*Department of Physics and Astronomy, The Johns Hopkins University,*

*3400 North Charles Street, Baltimore, MD 21218-2686, USA*

(Received 2004 April 12; accepted 2004 June 25)

## Abstract

In this paper, we focus on ram-pressure stripping and evaporation of disk galaxies in and around a cluster. We show that the evolution of the disk surface density affects the efficiency of ram-pressure stripping of galaxies at  $z \gtrsim 1$ . We also consider the saturation of thermal conduction in detail and show that it cannot be ignored at larger radii of a cluster, which makes the time-scale of the evaporation larger. Both the ram-pressure stripping and evaporation could affect the evolution of galaxies even around a cluster. In particular, the observed gradual decline of the star-formation rates of galaxies in and around clusters could be explained by evaporation without resorting to speculative strangulation (stripping of warm gas in galactic halos).

**Key words:** galaxies: clusters: general—galaxies: evolution—galaxies: high-redshift—galaxies: interactions

## 1. Introduction

Clusters of galaxies in the redshift range of 0.2–0.5 often exhibit an overabundance, relative to present-day clusters, of blue galaxies (Butcher, Oemler 1978, 1984). This star-formation activity is often called the Butcher–Oemler effect. Subsequent studies have confirmed this trend (Couch, Sharples 1987; Rakos, Schombert 1995; Lubin 1996; Margoniner, de Carvalho 2000; Ellingson et al. 2001; Goto et al. 2003a).

On the other hand, a correlation has been known between galaxy morphology and the local environment. Dressler (1980) studied 55 nearby galaxy clusters and found that fractions of early-type galaxies increase and those of late-type galaxies decrease with increasing local galaxy density in the clusters. Subsequent studies have confirmed the morphology–density relation, that is, early-type galaxies are dominated in inner region of clusters where the density is high and the fraction decreases toward the outside of the clusters (Whitmore, Gilmore 1991; Whitmore et al. 1993).

Recently, we have gradually understood that the above phenomena are related to each other. Dressler et al. (1994) and Couch et al. (1998) found that most of the blue galaxies observed as the Butcher–Oemler effect are normal spirals with active star formation. Dressler et al. (1997) studied 10 clusters at  $z \sim 0.5$ , and found the morphology–density relation at these redshifts. However, they also found that S0 fractions are much smaller than those in nearby clusters. The low fractions of S0 galaxies have also been observed by others (Fasano et al. 2000). In many clusters, their galaxy population gradually changes from a red, evolved, early-type population in the inner part of the clusters to a progressively blue, later-type population in the extensive outer envelope of the clusters (Abraham et al. 1996; Balogh et al. 1997; Rakos et al. 1997; Oemler et al. 1997; Smail et al. 1998; Couch et al. 1998; van Dokkum et al. 1998; Goto et al. 2004). These observations suggest that the blue, normal spirals observed in high-redshift clusters were originally field galaxies; they fell into clusters and evolved into the non-blue S0 galaxies observed in nearby clusters.

Several mechanisms have been proposed that can lead to color and morphological transformations between galaxy classes in clusters, such as, galaxy mergers (Toomre, Toomre 1972), tides from the cluster potential (Byrd, Valtonen 1990; Fujita 1998), tidal interactions between galaxies (Moore et al. 1996), ram-pressure stripping (Gunn, Gott 1972; Takeda et al. 1984; Gaetz et al. 1987; Portnoy et al. 1993; Balsara et al. 1994; Fujita, Nagashima 1999; Fujita et al. 1999; Abadi et al. 1999; Mori, Burkert 2000; Fujita 2001a), evaporation (Cowie, Songaila 1977), and a gradual decline in the star-formation rate of a galaxy owing to the stripping of halo gas (strangulation or suffocation; Larson et al. 1980; Kodama et al. 2001; Bekki et al. 2002).

In this paper, we focus on ram-pressure stripping and evaporation following Fujita (2004, hereafter Paper I). We mostly consider the star-formation history of galaxies, and do not treat the morphological transition in detail. We consider the redshift evolution of the disk-size and the surface density, which were not considered in Paper I. Moreover, we consider the evaporation in detail, while paying attention to the saturation of thermal conduction. We mainly treat the environmental effects on galaxies during the first infall into a cluster; we do not consider their long-term evolution. Thus, the high-redshift galaxies we investigate may not be direct progenitors of galaxies at  $z \sim 0$ . Although we often use the word ‘evolution’ from now on, it does not mean the evolution of ‘a particular galaxy’. Instead, we discuss the differences of the

average properties of galaxies at low and high redshifts. Although the models presented in this paper could be included in complicated semi-analytic models of galaxy formation, it would be instructive to study the characteristics of the environmental effects using simple models before we consider such a semi-analytic approach.

This paper is organized as follows. In section 2, we summarize our models. In section 3 we give the results of our calculations, and compare them with observations in section 4. Conclusions are given in section 5. As a cosmological model, we consider a cold dark-matter model with a non-zero cosmological constant ( $\Lambda$ CDM model). The cosmological parameters are  $h = 0.7$ , where the Hubble constant is given by  $H_0 = 100h \text{ km s}^{-1} \text{ Mpc}^{-1}$ ,  $\Omega_0 = 0.25$ ,  $\lambda_0 = 0.75$ , and  $\sigma_8 = 0.8$ .

## 2. Models

### 2.1. The Growth of Clusters

The typical mass of progenitors of a cluster can be derived from the extended Press–Schechter model (EPS) (Bower 1991; Bond et al. 1991; Lacey, Cole 1993) and its further extension (Fujita et al. 2002). The latter is a Press–Schechter model including the effect of spatial correlations among initial density fluctuations (SPS). The models are summarized in Paper I.

Cluster progenitors can be classified into two categories: one is the main cluster and the others are subclusters. The main cluster is the progenitor that was located near to the center of the current cluster, and had a much larger mass than the other progenitors. Subclusters are progenitors other than the main cluster that were located in the vicinity of the main cluster. Since the SPS model includes information about the spatial correlation of the initial density fluctuations of the universe, we can separately derive the typical masses of the main cluster and the subclusters. Moreover, the SPS model includes the EPS model. As shown in Paper I, we can define the typical mass of the main cluster at redshift  $z$ , which becomes a cluster of mass  $M_0$  at a later time,  $z_0 (< z)$ , as

$$\bar{M}_{\text{EPS}}(z|M_0, z_0) = \frac{\int_{M_{\min}}^{M_0} M P_{\text{EPS}}(M, z|M_0, z_0) dM}{\int_{M_{\min}}^{M_0} P_{\text{EPS}}(M, z|M_0, z_0) dM}, \quad (1)$$

where  $M_{\min}$  is the lower cutoff mass, and  $P_{\text{EPS}}(M, z|M_0, z_0)$  is the conditional probability based on the EPS model that a particle that resides in an object (‘halo’) of mass  $M_0$  at redshift  $z_0$  is contained in a smaller halo of mass  $M \sim M_1 + dM$  at redshift  $z$  ( $z > z_0$ ). We choose  $M_{\min} = 10^8 M_{\odot}$ , which corresponds to the mass of dwarf galaxies. The definition of  $P_{\text{EPS}}$  is shown in equation (8) in Paper I.

The typical mass of the subclusters is given by

$$\bar{M}_{\text{SPS}}(z|M_0, z_0) = \frac{\int_{M_{\min}}^{M_0} M P_{\text{SPS}}(M, z|M_0, z_0) dM}{\int_{M_{\min}}^{M_0} P_{\text{SPS}}(M, z|M_0, z_0) dM}, \quad (2)$$

where  $P_{\text{SPS}}(M, z | M_0, z_0)$  is the conditional probability based on the SPS model. The definition of  $P_{\text{SPS}}$  is shown in equation (7) in Paper I. We define the radius of the region that later becomes a cluster of mass  $M_0$  at  $z = z_0$  as  $R_0$ . Following Paper I, we consider the subclusters that were initially located at  $0.7R_0 < r < R_0$  in the precluster region. We refer to the inner radius as  $R_{\text{in}}$ .

## 2.2. Ram-Pressure Stripping

We adopt the ram-pressure stripping model of Paper I. In the following sections, we often refer to a relatively large dark halo containing galaxies and gas as a ‘cluster’. This ‘cluster’ includes the main cluster, the subclusters, and so on.

We assume that a cluster is spherically symmetric and the density distribution of the dark matter is

$$\rho_{\text{m}}(r) = \rho_{\text{mv}}(r/r_{\text{vir}})^{-a}, \quad (3)$$

where  $\rho_{\text{mv}}$  and  $a$  are constants,  $r_{\text{vir}}$  is the virial radius of the cluster, and  $r$  is the distance from the cluster center. We choose  $a = 2.4$  and determine  $\rho_{\text{mv}}$  and  $r_{\text{vir}}$  by a spherical collapse model following Paper I. We note that the average mass density of a cluster increases toward high redshift. For example, it is proportional to  $(1+z)^3$  for the Einstein–de Sitter universe.

We ignore the self-gravity of the ICM, and consider two ICM mass distributions. When the ICM is not heated by anything other than the gravity of the cluster, the distribution is written as

$$\rho_{\text{ICM}}(r) = \rho_{\text{ICM, vir}} \frac{[1 + (r/r_{\text{c}})^2]^{-a/2}}{[1 + (r_{\text{vir}}/r_{\text{c}})^2]^{-a/2}}, \quad (4)$$

where  $r_{\text{c}}/r_{\text{vir}} = 0.1$ . We call this model ‘the non-heated ICM model’. In this model, we assume that the ICM temperature equals to the virial temperature ( $T_{\text{ICM}} = T_{\text{vir}}$ ).

However, at least for nearby clusters and groups, an entropy excess of the ICM (an entropy floor) has been observed in X-rays in the central regions. This indicates that the ICM has been heated by some sources, such as AGNs or supernovae, in addition to the gravity of the clusters and groups (Ponman et al. 1999; Lloyd-Davies et al. 2000; Mulchaey 2000; Mulchaey et al. 2003). Thus, we construct ‘the heated ICM model’. We assume that the ICM is heated before cluster formation. Although there is a debate about whether the heating took place before or after cluster formation (Fujita 2001b; Yamada, Fujita 2001; Babul et al. 2002; Voit et al. 2002), the following results would not be much different, even if the ICM is heated after cluster formation (Loewenstein 2000). If the ICM is heated non-gravitationally before cluster formation, the final distribution depends on the virial temperature of the cluster,  $T_{\text{vir}}$ . If  $T_{\text{vir}} \geq T_0$ , we assume that a shock forms near the virial radius of the cluster. In this study, we assume  $T_0 = 0.8$  keV from X-ray observations (Fujita, Takahara 2000; Paper I). The ICM distribution is given by

$$\rho_{\text{ICM}}(r) = \rho_{\text{ICM, vir}} \frac{[1 + (r/r_{\text{c}})^2]^{-3b/2}}{[1 + (r_{\text{vir}}/r_{\text{c}})^2]^{-3b/2}}, \quad (5)$$

where  $b = (2.4/3)T_{\text{vir}}/T_{\text{ICM}}$  and  $T_{\text{ICM}}$  is the temperature of the ICM, which is given by  $T_{\text{ICM}} = T_{\text{vir}} + T_0$ . If  $T_{\text{vir}} < T_0$  keV, a shock does not form, but the gas accreted by a cluster adiabatically falls into the cluster. The ICM density and temperature profiles are approximately given by

$$\rho_{\text{ICM}}(r) = \rho_{\text{ICM,vir}} \left[ 1 + \frac{3}{A} \ln \left( \frac{r_{\text{vir}}}{r} \right) \right]^{3/2}, \quad (6)$$

$$T_{\text{ICM}}(r) = \frac{4}{15} \left[ 1 + \frac{3}{A} \ln \left( \frac{r_{\text{vir}}}{r} \right) \right], \quad (7)$$

where  $A$  is the constant determined by the adiabat of the ICM (Balogh et al. 1999a; Paper I). Since equations (6) and (7) diverge at  $r = 0$ , we take their values at  $r = 0.1r_{\text{vir}}$  as the central values. In equations (4), (5), and (6), the normalizations of the ICM profile are given by the observed ICM fraction of clusters or the rate of gas accretion to clusters (Paper I). If the non-gravitational heating makes the accretion time larger than the lifetime of a cluster, the cluster cannot accrete much gas and the gas fraction is smaller than the average in the universe. This happens at high redshifts ( $z \gtrsim 1-2$ ) in our models.

We consider a radially infalling disk galaxy from the turnaround radius of a cluster ( $2r_{\text{vir}}$ ). As the velocity of the galaxy increases, the ram-pressure from the ICM also increases. The condition of ram-pressure stripping is

$$\begin{aligned} \rho_{\text{ICM}} v_{\text{rel}}^2 &> 2\pi G \Sigma_{\star} \Sigma_{\text{HI}} \\ &= v_{\text{rot}}^2 r_{\text{gal}}^{-1} \Sigma_{\text{HI}} \\ &= 2.1 \times 10^{-11} \text{dyn cm}^{-2} \left( \frac{v_{\text{rot}}}{220 \text{ km s}^{-1}} \right)^2 \\ &\quad \times \left( \frac{r_{\text{gal}}}{10 \text{ kpc}} \right)^{-1} \left( \frac{\Sigma_{\text{HI}}}{8 \times 10^{20} m_{\text{H}} \text{ cm}^{-2}} \right), \end{aligned} \quad (8)$$

where  $v_{\text{rel}}$  is the relative velocity between the galaxy and the ICM,  $\Sigma_{\star}$  is the gravitational surface mass density,  $\Sigma_{\text{HI}}$  is the surface density of the HI gas,  $v_{\text{rot}}$  is the rotation velocity, and  $r_{\text{gal}}$  is the characteristic radius of the galaxy (Gunn, Gott 1972; Fujita, Nagashima 1999). We define the cluster radius at which condition (8) is satisfied for the first time as the stripping radius,  $r_{\text{st}}$ . Since we assume that the ICM is nearly in pressure equilibrium for  $r < r_{\text{vir}}$ , the relative velocity,  $v_{\text{rel}}$ , is equivalent to the velocity of the galaxy relative to the cluster,  $v$ , for  $r < r_{\text{vir}}$ .

### 2.3. Evaporation

The time-scale of the evaporation of cold gas in a galaxy is written as

$$t_{\text{cond}} \approx \frac{3}{2} \frac{k_{\text{B}} T_{\text{ICM}}}{\mu m_{\text{H}}} \frac{M_{\text{cold}}}{|L|}, \quad (9)$$

where  $k_{\text{B}}$  is the Boltzmann constant,  $T_{\text{ICM}}$  is the ICM temperature,  $\mu$  ( $=0.6$ ) is the mean molecular weight,  $m_{\text{H}}$  is the hydrogen mass,  $M_{\text{cold}}$  is the mass of cold gas in the galaxy, and  $L$  is the energy flux from the hot ICM surrounding the galaxy via thermal conduction (Paper I).

We define neutral and molecular gas confined in a galactic disk as cold gas; we do not consider the cold gas in a galactic bulge. If the electron mean-free path is smaller than the spatial scale of the temperature gradient around the galaxy, the thermal conduction is not saturated and the energy flux is given by

$$|L_{\text{nsat}}| = 4\pi r_{\text{gal}}^2 \kappa_0 T_{\text{ICM}}^{7/2}, \quad (10)$$

where  $r_{\text{gal}}$  is the galaxy radius, and  $\kappa_0 = 5 \times 10^{-7} \text{ erg cm}^{-1} \text{ s}^{-1} \text{ K}^{-3.5}$  (Paper I). If the electron mean-free path is larger than the spatial scale of the temperature gradient, the thermal conduction is saturated and the energy flux is given by

$$|L_{\text{sat}}| = 4\pi r_{\text{gal}}^2 \times 0.4 n_e k_B T_{\text{ICM}} \left( \frac{2k_B T_{\text{ICM}}}{\pi m_e} \right)^{1/2}, \quad (11)$$

where  $n_e$  is the electron number density, and  $m_e$  is the electron mass (Cowie, McKee 1977). For convenience, we often refer to  $t_{\text{cond}}$  given by  $L = L_{\text{nsat}}$  as  $t_{\text{cond,nsat}}$  and that given by  $L = L_{\text{sat}}$  as  $t_{\text{cond,sat}}$ . An actual energy flux is given by  $|L| = \min(|L_{\text{nsat}}|, |L_{\text{sat}}|)$ .

#### 2.4. Evolution of Disk Properties

The most important difference between this study and Paper I is that we consider the redshift evolution of disk properties in this paper. We adopted a simple model, discussed in Mo et al. (1998), for the galactic disk.

For a given rotation velocity, the galaxy radius at redshift  $z$  is given by

$$r_{\text{gal}}(z) = r_{\text{gal},0} (H[z]/H_0)^{-1}, \quad (12)$$

where  $r_{\text{gal},0}$  is the galaxy radius at  $z = 0$  and

$$H(z) = H_0 [\lambda_0 + (1 - \lambda_0 - \Omega_0)(1 + z)^2 + \Omega_0(1 + z)^3]^{1/2} \quad (13)$$

is the Hubble constant at redshift  $z$ . The surface density and mass of the disk at redshift  $z$  are given by

$$\Sigma_{\star}(z) = \Sigma_{\star,0} H(z)/H_0, \quad (14)$$

$$M_{\text{disk}}(z) = M_{\text{disk},0} (H[z]/H_0)^{-1}, \quad (15)$$

where  $\Sigma_{\star,0}$  and  $M_{\text{disk},0}$  are the surface density and mass at  $z = 0$ , respectively. As shown in figure 1 in Mo et al. (1998),  $H(z = 1) \sim 2H_0$ . Thus, the disk radius (surface density) at  $z \sim 1$  is a factor of two smaller (larger) than that at  $z = 0$ .

We give the column density of the HI gas in the disk and the mass of the cold gas *before* the galaxy is affected by environmental effects as follows. We assume that  $\Sigma_{\text{HI}} \propto \Sigma_{\star}$  for simplicity; in the future study, we will not assume this by using a semi-analytic model of galaxy formation. Thus, the column density of the HI gas at redshift  $z$  is given by

$$\Sigma_{\text{HI}}(z) = \Sigma_{\text{HI},0} H(z)/H_0, \quad (16)$$

where  $\Sigma_{\text{HI},0}$  is the column density at  $z = 0$ . We also assume that  $M_{\text{cold}} \propto M_{\text{disk}}$  and

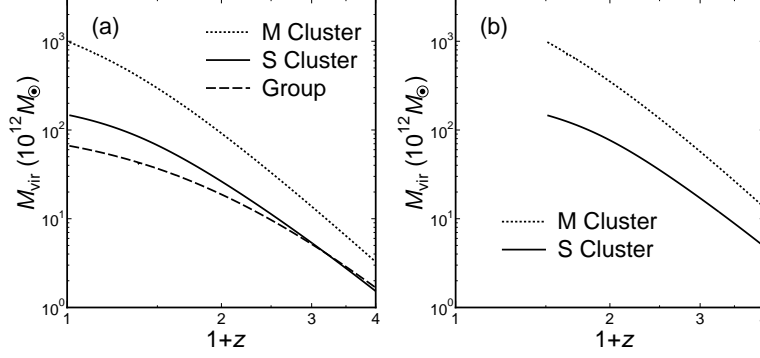


**Fig. 1.** (a) Mass evolution of the main cluster (dotted line), the typical subcluster (solid line) of the LCL, and the group (dashed line). (b) Mass evolution of the main cluster (dotted line) and the typical subcluster (solid line) of the HCL.

$$M_{\text{cold}}(z) = M_{\text{cold},0} (H[z]/H_0)^{-1}, \quad (17)$$

where  $M_{\text{cold},0}$  is the mass of the cold gas at  $z = 0$ .

### 3. Results

We considered the evolution of clusters with three masses at  $z = z_0$ . Two of them are the same as those in Paper I. The masses of the two clusters at  $z_0 = 0$  are  $M_0 = 1 \times 10^{15} M_\odot$  and  $6.7 \times 10^{13} M_\odot$ . We call the former cluster ‘the low-redshift cluster (LCL)’, which is studied to be compared with clusters observed at  $z \sim 0.5$ . Actually, at  $z = 0.5$ , the mass of the main cluster is  $M_{\text{vir}} = 3 \times 10^{14} M_\odot$ , which is close to the masses of well-known clusters observed at  $z \sim 0.5$  (Schindler 1999). The typical mass of the subclusters of the LCL at  $z = 0.5$  is  $M_{\text{vir}} = 6.7 \times 10^{13} M_\odot$  (figure 1). The latter cluster with  $M_0 = 6.7 \times 10^{13} M_\odot$  at  $z_0 = 0$  is investigated to be compared with the subclusters. Since the mass scale of this cluster is that of groups of galaxies, we call this cluster ‘the group’. For the group, we considered only the evolution of the main cluster. The third cluster that we studied has a mass of  $M_0 = 1 \times 10^{15} M_\odot$  at  $z_0 = 0.5$ . This cluster was studied to be compared with recent observations of clusters observed at  $0.5 \lesssim z \lesssim 1$ . We call this cluster ‘the high-redshift cluster (HCL)’.

In figure 1, we present the evolutions of the cluster masses. We expect that when the mass of the main cluster satisfies the relation  $M_{\text{vir}}/M_0 = (R_{\text{in}}/R_0)^3$ , the subclusters begin to be included in the main cluster and become subhalos. For the parameters we adopted (e.g.,  $R_{\text{in}} = 0.7R_0$ ), the subclusters of the LCL and HCL are absorbed by the main clusters, together with the galaxies in them, at  $z \lesssim 0.4$  and 1, respectively. This means that at  $z \sim 0.4$  (1) the subclusters of the LCL (HCL) are to be observed just outside the main cluster of the LCL (HCL).

Since we are interested in galaxies at high redshift, we investigated relatively large galaxies that can be observed in detail. We consider two model galaxies following Paper I. While



we fixed the rotation velocities of the galaxies  $v_{\text{rot}}$ , we changed the radius, surface density, and HI column density according to equations (12), (14), and (16). The parameters for the bigger model galaxy, which is similar to the Milky Way, are  $v_{\text{rot}} = 220 \text{ km s}^{-1}$ ,  $r_{\text{gal},0} = 10 \text{ kpc}$ , and  $\Sigma_{\text{HI},0} = 8 \times 10^{20} m_{\text{H}} \text{ cm}^{-2}$ . The parameters for the smaller model galaxy, which is similar to M33, are  $v_{\text{rot}} = 105 \text{ km s}^{-1}$ ,  $r_{\text{gal},0} = 5 \text{ kpc}$ , and  $\Sigma_{\text{HI},0} = 14 \times 10^{20} m_{\text{H}} \text{ cm}^{-2}$ . These are the values at  $z = 0$  even for the galaxies in the HCL. From now on, this disk evolution is considered unless otherwise mentioned.

### 3.1. Ram-Pressure Stripping

First, we consider the time-scale of ram-pressure stripping. Although equation (8) is the condition at the representative radius of a galaxy, numerical simulations performed by Abadi, Moore, and Bower (1999) showed that it can also be applied at ‘each radius’ of the galaxy. Assuming that  $v_{\text{rot}}$  is the constant and  $\Sigma_{\text{HI}} \propto \Sigma_{\star}$ , the HI column density has the relation  $\Sigma_{\text{HI}} \propto \Sigma_{\star} \propto v_{\text{rot}}^2 / \tilde{r} \propto \tilde{r}^{-1}$ , where  $\tilde{r}$  is the distance from the galaxy center. Thus, equation (8) shows that the ram-pressure required for stripping at  $\tilde{r} = 5 \text{ kpc}$  is 4-times larger than that at  $\tilde{r} = 10 \text{ kpc}$ . Figure 2 shows the time elapsed since the cold gas at  $\tilde{r} = 10 \text{ kpc}$  is stripped until that at  $\tilde{r} = 5 \text{ kpc}$  is stripped,  $\Delta t_{10-5}$ , for the radially infalling bigger galaxy ( $v_{\text{rot}} = 220 \text{ km s}^{-1}$ ). For  $\tilde{r} \lesssim 5 \text{ kpc}$ , the effect of the galactic bulge would be important; since we are interested in the star-formation activities in galactic disks, we ignore the inner regions. For a comparison, the rotation time of the galaxy at  $\tilde{r} = 10 \text{ kpc}$  is shown in figure 2. The minimum time-scale of the evolution of a galaxy is expected to be the rotation time ( $t_{\text{rot}}$ ). For example, the passage of a galactic arm through a molecular cloud could stimulate star formation. Thus, if  $\Delta t_{10-5} \lesssim t_{\text{rot}}$ , the ram-pressure stripping can be regarded as an instantaneous phenomenon for the galaxy, which is the case for our model galaxy (figure 2). Thus, the long-term evolution of the galaxy does not need to be considered. Moreover,  $\Delta t_{10-5}$  is much smaller than the crossing time of the galaxy in the cluster. If turbulent and viscous stripping is considered, the stripping could be even faster (Quilis et al. 2000). Since the  $\rho_{\text{ICM}}$  and  $v_{\text{rel}}$  rapidly decrease as the distance from the cluster center increases, the ram-pressure becomes less effective in the outer region of the cluster. Thus, at cluster radii  $r > r_{\text{st}}$ , where  $r_{\text{st}}$  is defined by the pressure balance at the galactic radius  $\tilde{r} = r_{\text{gal}}$  [equation (8)], it is unlikely that the ram-pressure directly affects the evolution of the galactic disk. Although galactic gas at  $\tilde{r} > r_{\text{gal}}$  might be affected by ram-pressure at  $r > r_{\text{st}}$ , the effect should be included in ‘strangulation’, which is considered in Paper I.

Since cold gas in a galactic disk is almost instantaneously stripped by ram-pressure,  $r_{\text{st}}/r_{\text{vir}}$  should be related to the fraction of galaxies affected by ram-pressure stripping in a cluster. The evolutions of  $r_{\text{st}}/r_{\text{vir}}$  are shown in figures 3 (the bigger galaxy) and 4 (the smaller galaxy). Compared to the non-heated ICM model,  $r_{\text{st}}/r_{\text{vir}}$  decreases faster toward higher redshift in the heated ICM model. This is because the non-gravitational heating reduces the ICM density and the ram-pressure on galaxies in the inner part of a cluster. In the heated



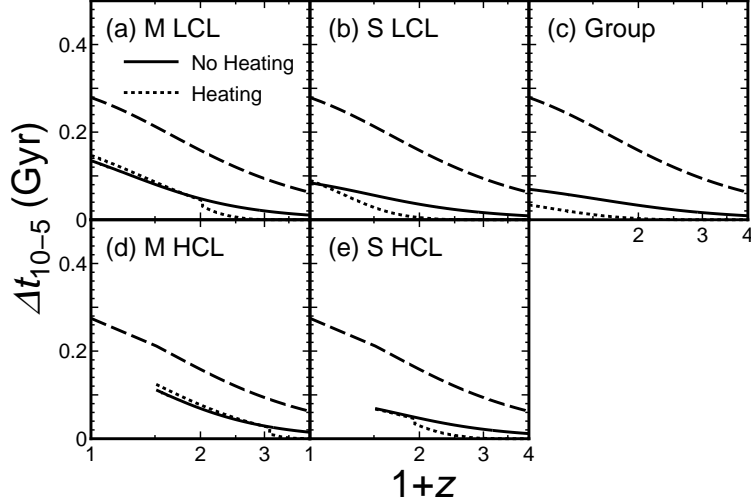


**Fig. 2.** Time-scale of ram-pressure stripping,  $\Delta t_{10-5}$  for the bigger galaxy in the (a) main cluster of the LCL, (b) subcluster of the LCL, (c) group, (d) main cluster of the HCL, and (e) subcluster of the HCL. The solid lines are the results of the non-heated ICM model and the dotted lines are those of the heated ICM model. The dashed-line shows the rotation time of the galaxy ( $t_{\text{rot}}$ ).

ICM models, the changes of the slopes correspond to the transformations of the assumed ICM distributions (see Paper I). The differences between figures 3 and 4 are small, which shows that the differences of the galaxy properties do not much affect the ram-pressure stripping. Of course, for much smaller galaxies,  $r/r_{\text{st}}$  should be much different from those in figures 3 and 4. However, those small galaxies are difficult to be observed in detail at high redshifts.

In figures 3 and 4, we also present the evolutions when the disk properties do not evolve, which were shown in figures 2 and 3 in Paper I; for  $z \lesssim 0.5$ , when the disk properties evolve,  $r_{\text{st}}/r_{\text{vir}}$  is not much different from that when they do not evolve. For  $z \gtrsim 1$ , however, the former is much smaller than the latter. This is because in the former case, the surface density of the disk is larger at a higher redshift, and the disk is more robust against ram-pressure stripping [equation (14)]. As discussed in Fujita (2001a), the ram-pressure from the ICM is larger at higher redshifts, because the average mass density of clusters at higher redshifts is larger than that of clusters at lower redshifts. Thus, the results show that the effect of the larger disk surface density dominates that of the larger ram-pressure at high redshifts.

For the HCL,  $r_{\text{st}}/r_{\text{vir}}$  is larger than that for the LCL for a given redshift, because the mass of the HCL is larger than that of the LCL, and the typical galaxy velocity in the HCL is larger than that in the LCL (Paper I). On the other hand, for a given mass, ram-pressure stripping is more effective in higher redshift clusters. The mass of the main cluster of the HCL at  $z \sim 1$  is almost the same as that of the LCL at  $z \sim 0.5$  ( $\sim 3 \times 10^{14} M_{\odot}$ ; figure 1). However,  $r_{\text{st}}/r_{\text{vir}}$  is larger and ram-pressure stripping is more effective in the former.

Tormen, Moscardini, and Yoshida (2004) studied the orbital properties of galaxies in

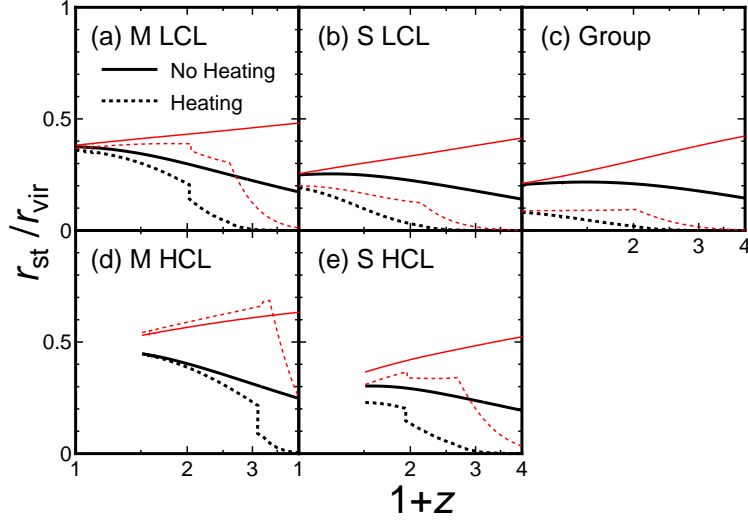


**Fig. 3.** Evolution of the stripping radii,  $r_{st}$ , normalized by the virial radii,  $r_{vir}$ , for the bigger galaxy in the (a) main cluster of the LCL, (b) subcluster of the LCL, (c) group, (d) main cluster of the HCL, and (e) subcluster of the HCL. Solid lines are the results of the non-heated ICM model and dotted lines are those of the heated ICM model. Bold and thin lines are those when the evolution of a galactic disk is considered and those when it is not considered, respectively. For  $r < r_{st}$ , ram-pressure stripping is effective.

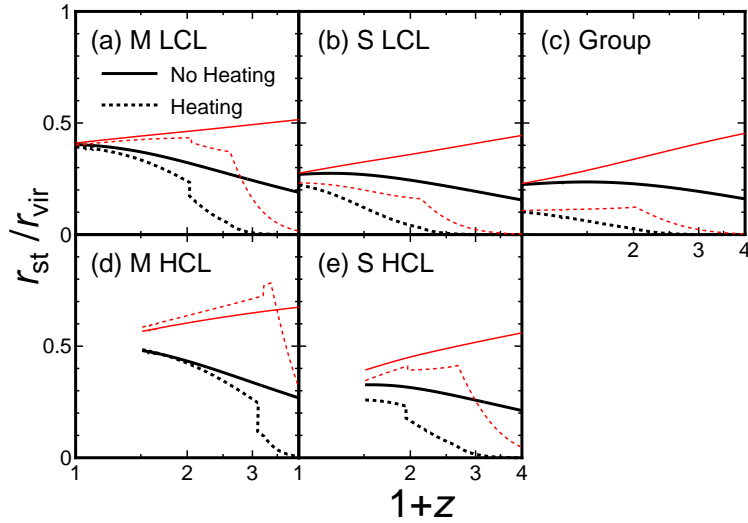


**Fig. 4.** Same as figure 3, but for the smaller galaxy.

massive clusters at  $z < 0.8$  by numerical simulations. Since they showed that the typical pericentric radius of galaxies for the first passage is about  $0.3r_{\text{vir}}$ , ram-pressure stripping is effective if  $r_{\text{st}}/r_{\text{vir}} \gtrsim 0.3$ . Here, we assume that the results of Tormen, Moscardini, and Yoshida (2004) can be applied to our model clusters and the progenitors. If the disk evolution is considered and non-gravitational heating is not considered, ram-pressure stripping is effective at  $z \lesssim 1$  for the main cluster of the LCL,  $z \lesssim 2.5$  for the main cluster of the HCL, and  $z \lesssim 1$  for the subclusters of the HCL, while it is not effective for the subclusters of LCL and the group regardless of  $z$  (figures 3 and 4). Figures 3 and 4 also show that if both the disk evolution and non-gravitational heating are considered, ram-pressure stripping is effective at  $z \lesssim 0.5$  for the main cluster of the LCL, and  $z \lesssim 1.5$  for the main cluster of the HCL, while it is not effective for the subclusters of the LCL and HCL, and the group regardless of  $z$ . We note that in Paper I the tidal force from the main cluster and the resultant shift of the orbit of a galaxy in the subcluster are estimated; the estimated pericentric radius of the galaxy is  $\sim 0.2r_{\text{vir}}$ . Thus, the assumed threshold of ram-pressure stripping ( $r_{\text{st}}/r_{\text{vir}} \lesssim 0.3$ ) seems to be reasonable even for the subclusters. For the subclusters of the LCL, for example, since  $0.2 \lesssim r_{\text{st}}/r_{\text{vir}} \lesssim 0.3$  at  $z \lesssim 1$  in the non-heated ICM model, we should rather say that the ram-pressure stripping is marginally effective at  $z \lesssim 1$  in the non-heated ICM model.

### 3.2. Evaporation

In Paper I, we mainly investigated the evaporation effect on galaxies in clusters (or the progenitors) that have not been heated non-gravitationally. In this study, we also focus on the evaporation in clusters that have been heated non-gravitationally. Moreover, we study the saturation effect of thermal conduction on the evaporation time-scale in detail. Following Paper I, we assume that  $M_{\text{cold},0} = 5 \times 10^9 M_{\odot}$  for the bigger galaxy, and  $M_{\text{cold},0} = 4 \times 10^9 M_{\odot}$  for the smaller galaxy.

In figures 5 and 6, we present  $t_{\text{cond,nsat}}$  and  $t_{\text{cond,sat}}$  at  $r = 0$  and  $r_{\text{vir}}$  for the bigger galaxy; figure 5 is for the non-heated ICM model, and figure 6 is for the heated ICM model. Note that since  $t_{\text{cond,nsat}} \propto M_{\text{cold}}/r_{\text{gal}}$  for the unsaturated case and  $t_{\text{cond,sat}} \propto M_{\text{cold}}/r_{\text{gal}}^2$  for the saturated case [equations (9), (10), and (11)],  $t_{\text{cond,nsat}}$  ( $t_{\text{cond,sat}}$ ) for the smaller galaxy is 1.6 (3.2) times *larger* at a given redshift for our parameters. Thus, the differences between the bigger galaxy and the smaller galaxy do not much affect the following results. The actual evaporation time-scale of a galaxy at a radius  $r$  is given by  $t_{\text{cond}}(r) \equiv \max[t_{\text{cond,nsat}}(r), t_{\text{cond,sat}}(r)]$ . For example, at lower redshifts for the main cluster of the LCL, the saturation cannot be ignored at  $r = r_{\text{vir}}$  and  $t_{\text{cond}} = t_{\text{cond,sat}}$ .

In the non-heated ICM model,  $t_{\text{cond,nsat}}$  increases as  $z$  increases because  $t_{\text{cond,nsat}} \propto T_{\text{ICM}}^{-5/2}$  and  $T_{\text{ICM}}$  decreases rapidly with the mass of the cluster progenitors [equations (9) and (10)]. In the non-heated ICM model,  $t_{\text{cond,sat}}(r = 0)$  and  $t_{\text{cond,sat}}(r = r_{\text{vir}})$  decrease slowly as  $z$  increases (figure 5). This is because their  $T_{\text{ICM}}$ -dependence is small ( $\propto T_{\text{ICM}}^{-1/2}$ ) and the increase of  $n_e$  at

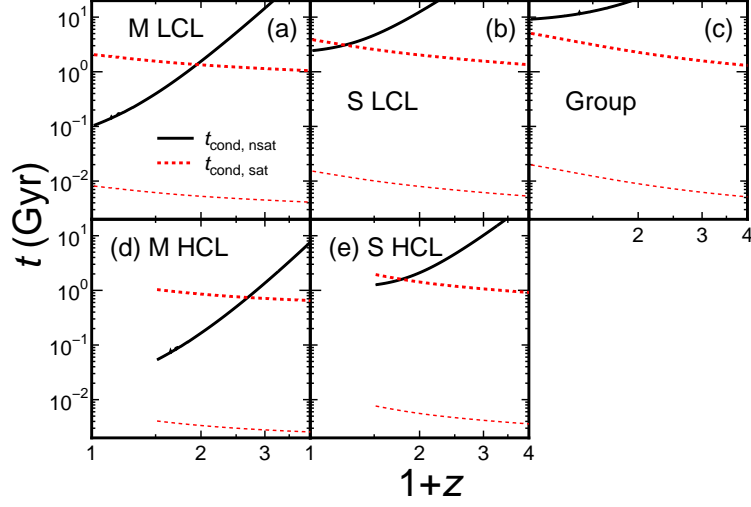


**Fig. 5.** Evolution of the conduction times for the non-heated ICM model for the bigger galaxy in the (a) main cluster of the LCL, (b) subcluster of the LCL, (c) group, (d) main cluster of the HCL, and (e) subcluster of the HCL. The solid lines are  $t_{\text{cond,nsat}}$  at  $r=0$  (thin lines) and  $r=r_{\text{vir}}$  (thick lines). The dotted lines are  $t_{\text{cond,sat}}$  at  $r=0$  (thin lines) and  $r=r_{\text{vir}}$  (thick lines). Note that  $t_{\text{cond,nsat}}(r=0) = t_{\text{cond,nsat}}(r_{\text{vir}})$  in this figure.

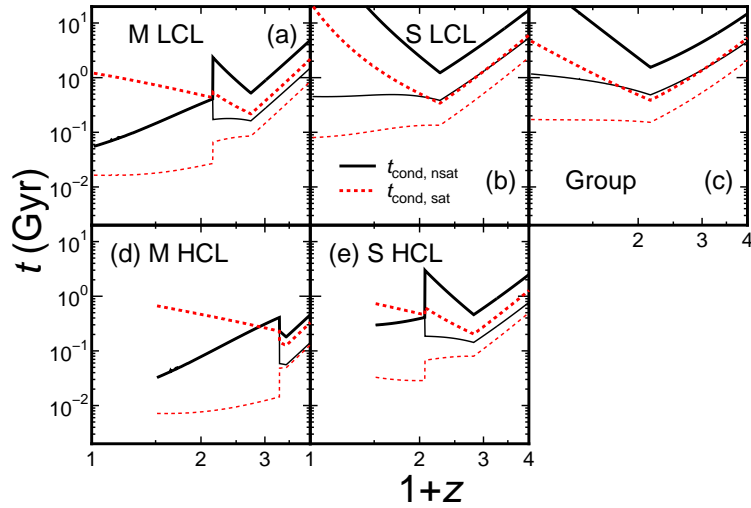


**Fig. 6.** Same as figure 5, but for the heated ICM model.

high redshift dominates [equations (9) and (11)].

In the heated ICM model, the evolution of the conduction time-scales is more complicated (figure 6). In general, the conduction time-scales in the heated ICM model are smaller than those in the non-heated ICM model because of larger  $T_{\text{ICM}}$  owing to non-gravitational heating. The detailed behavior of the conduction time-scale when thermal conduction is not saturated,  $t_{\text{cond,nsat}}$ , can be explained as follows. For the main clusters of the LCL and the HCL and the subcluster of the HCL,  $t_{\text{cond,nsat}}$  increases as  $z$  increases. This is because  $T_{\text{ICM}}$  decreases as is the case of the non-heated ICM model. However, the increasing rate is smaller because  $T_{\text{ICM}}$  decreases more slowly owing to non-gravitational heating. For higher redshifts, the virial temperature becomes smaller and satisfies the relation  $T_{\text{vir}} < T_0$ , where  $T_0$  ( $=0.8$  keV) is the critical temperature under which the ICM distribution follows an adiabatic accretion model (subsection 2.2). For example,  $T_{\text{vir}}$  equals  $T_0 = 0.8$  keV at  $z = 1.2$  for the main cluster of the LCL. Since the cluster is not isothermal in the adiabatic accretion model [equation (7)],  $t_{\text{cond,nsat}}$  bifurcates there. For the subcluster of the LCL and the group, the density and temperature profiles follow those predicated by the adiabatic accretion model for  $z \geq 0$ . In these redshift ranges,  $t_{\text{cond,nsat}}(r = r_{\text{vir}}) > t_{\text{cond,nsat}}(r = 0)$  because  $T_{\text{ICM}}(r = r_{\text{vir}}) < T_{\text{ICM}}(r = 0)$ . In the middle-redshift range,  $1.2 < z < 1.7$  for the main cluster of the LCL for example, the ICM fraction of a cluster is the same as that at lower redshift although the cluster is more compact at the higher redshifts. Therefore,  $T_{\text{ICM}}$  increases via adiabatic compression and  $t_{\text{cond,nsat}}(r = r_{\text{vir}})$  decreases as  $z$  increases. At higher redshifts,  $z > 1.7$  for the main cluster of the LCL for example,  $t_{\text{cond,nsat}}$  increases as  $z$  increases, because the ICM fraction and  $T_{\text{ICM}}$  decrease.

The behavior of the saturated conduction time-scale,  $t_{\text{cond,sat}}$ , at lower redshifts ( $z \lesssim 1.2$  for the main cluster of the LCL, for example) can be explained as follows. Since the average dark matter and ICM densities increase toward higher redshifts, the increase of  $t_{\text{cond,sat}}$  through the decrease of  $T_{\text{ICM}}$  is dominated by the decrease of  $t_{\text{cond,sat}}$  through the increase of  $n_e$  [equations (9) and (11)] at  $r = r_{\text{vir}}$ . However, in our ICM model, for a given gas mass fraction, the non-gravitational heating decreases the ICM density in the central region of a cluster. Thus, the decrease of  $t_{\text{cond,sat}}$  is not significant at  $r = 0$ . At higher redshifts, once the density and temperature profiles follow those predicted by the adiabatic accretion model, the behaviors of  $t_{\text{cond,sat}}$  can be attributed to the mechanisms that are the same as the case of  $t_{\text{cond,nsat}}$ .

In figure 7, we show the evolution of  $t_{\text{cond}} = \max(t_{\text{cond,nsat}}, t_{\text{cond,sat}})$  at  $r = 0$  for the bigger galaxy in the non-heated ICM model. This figure corresponds to figure 5 in Paper I in which the evolution of the disk is not taken into account. As shown in figure 5,  $t_{\text{cond,nsat}} \gg t_{\text{cond,sat}}(r = 0)$  and therefore  $t_{\text{cond}}(r = 0) = t_{\text{cond,nsat}}$ . The conduction time-scale can be represented by  $t_{\text{cond}} \propto M_{\text{cold}}/r_{\text{gal}}$  [equations (9) and (10)]. Since both  $M_{\text{cold}}$  and  $r_{\text{gal}}$  are proportional to  $H(z)^{-1}$  [equations (12) and (17)],  $t_{\text{cond}}$  is not influenced by the effect of the disk evolution. Thus, the upper figures are the same as figures 5a–c in Paper I. In figure 7, we also present the Hubble time,  $t_{\text{H}}$ . If  $t_{\text{cond}} \ll t_{\text{H}}$ , the cold gas in a galaxy is evaporated soon after the galaxy forms in

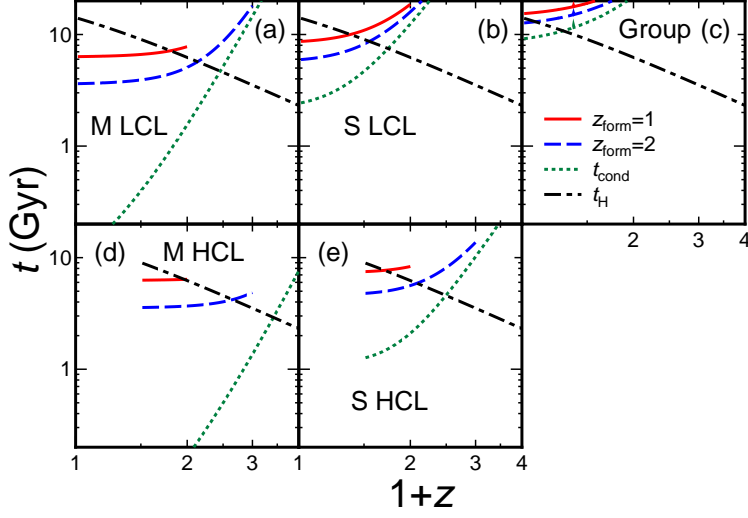


**Fig. 7.** Time-scales of thermal conduction,  $t_{\text{cond}}(r=0)$  for the non-heated ICM model for the bigger galaxy in the (a) main cluster of the LCL, (b) subcluster of the LCL, (c) group, (d) main cluster of the HCL, and (e) subcluster of the HCL. The solid and dashed lines show  $t_{\text{cond}}(r=0)' = t_{\text{cond}}(r=0) + t_{\text{form}}$  when  $z_{\text{form}} = 1$  and 2, respectively. The dotted and dot-dashed lines show  $t_{\text{cond}}(r=0)$  and the Hubble time  $t_{\text{H}}$ , respectively. For  $t'_{\text{cond}} \lesssim t_{\text{H}}$ , thermal conduction is effective.

the cluster or its progenitors. We also show  $t'_{\text{cond}}(r=0) = t_{\text{cond}}(r=0) + t_{\text{form}}$ , where  $t_{\text{form}}$  is the Hubble time when the galaxy forms at  $z = z_{\text{form}}$ . If  $t'_{\text{cond}} < t_{\text{H}}$  at a given redshift, the cold gas in the galaxy has been evaporated by the redshift. Note that  $t_{\text{cond}}$  corresponds to  $t'_{\text{cond}}$  when  $z_{\text{form}} = \infty$ .

Figure 7 shows that in the main cluster of the LCL (HCL) observed at  $z \sim 0.5$  (1), cold gas has been evaporated from the galaxies near the cluster center. On the other hand, in the subclusters of the LCL (HCL) observed at  $z \sim 0.5$  (1), cold gas is evaporating if the galaxies formed at  $z \sim 1$ –2. The time-scales of the evaporation,  $t_{\text{cond}}$ , is relatively long ( $\gtrsim 2$  Gyr). In the group, cold gas is evaporating at  $z \sim 0$ .

In figure 8, we present the evolutions of  $t_{\text{cond}}(r=0)$  and  $t'_{\text{cond}}(r=0)$  for the bigger galaxy in the heated ICM model. Since  $t_{\text{cond}}$  in the heated ICM model is generally smaller than that in the non-heated ICM owing to the larger  $T_{\text{ICM}}$ ,  $t'_{\text{cond}}$  becomes smaller than  $t_{\text{H}}$  soon after galaxy formation.

A galaxy that first enters a cluster from the outside does not stay at  $r = r_{\text{vir}}$  and the orbit is not exactly radial. If we assume that the typical peri-centric radius of galaxies is about  $0.3r_{\text{vir}}$ , ram-pressure stripping is effective for most galaxies if  $r_{\text{st}}/r_{\text{vir}} \gtrsim 0.3$  (see subsection 3.1). On the other hand, if  $r_{\text{st}}/r_{\text{vir}} \lesssim 0.3$ , the galaxies would be affected only by evaporation while they are orbiting. In this case, the actual time-scale of evaporation,  $t_{\text{evap}}$ , is given by  $t_{\text{cond}}(r=0) < t_{\text{evap}} < t_{\text{cond}}(r=r_{\text{vir}})$ . Therefore, in the subclusters of the LCL observed at  $z \sim 0.5$ , the bigger galaxy infalling from the outside loses its cold gas with a time-scale of  $0.5 < t_{\text{evap}} < 10$  Gyr

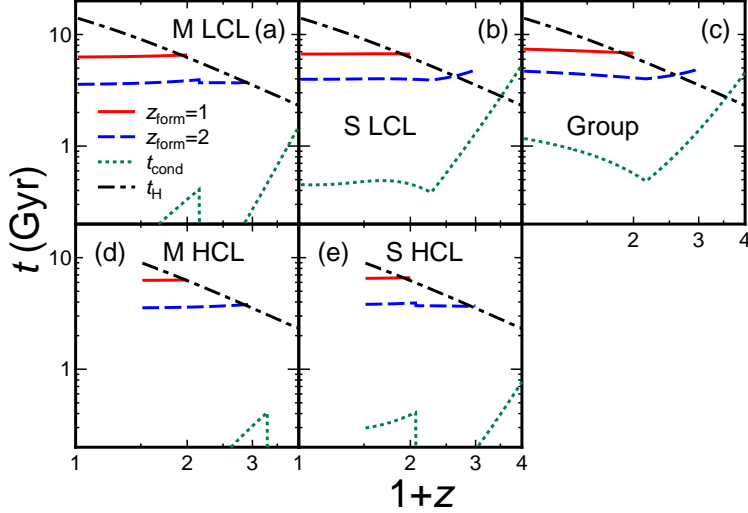


**Fig. 8.** Same for figure 7, but for the heated ICM model.

in the heated ICM model (figure 6). In the subclusters of the HCL observed at  $z \sim 1$ , a galaxy loses its cold gas with the time-scale of  $t_{\text{evap}} \sim 0.5$  Gyr in the heated ICM model (figure 6).

### 3.3. Comparison between Ram-pressure Stripping and Evaporation

Although both ram-pressure stripping and evaporation suppress star-formation activities in galaxies, they affect the star-formation activities differently. For position, while the ram-pressure stripping is effective only in the central regions of clusters ( $r \lesssim 0.5r_{\text{vir}}$ ; figures 3 and 4), the evaporation is often effective even at  $r \sim r_{\text{vir}}$ . For time-scale, while the ram-pressure stripping checks star-formation activities in a very short time ( $\sim 10^8$  yr; figure 2, see Fujita, Nagashima 1999), the evaporation generally affects the star-formation activities more slowly ( $\sim 10^9$  yr; figures 5 and 6). The difference in the decline rate of the star-formation activities could be discriminated by the spectra of the galaxies. These facts would be useful to observationally find whether ram-pressure stripping or evaporation dominates in clusters. In the next section, we investigate several specific cases.

## 4. Discussion

In Paper I, the star-formation activities of galaxies in main clusters and the subclusters in the vicinity of the main clusters observed at  $z \sim 0.5$  are discussed. Since the consideration of the disk evolution does not much change  $r_{\text{st}}/r_{\text{vir}}$  for  $z \lesssim 0.5$  for the LCL (figures 3 and 4), the conclusions about the effects of ram-pressure stripping on the galaxies do not change either. In Paper I, we discussed that the rapid decline of the star-formation rates of galaxies in the main cluster of the LCL is not consistent with observations of the CNOC sample of very luminous X-ray clusters (Balogh et al. 1999b; Kodama, Bower 2001) and this suggests that the star-formation rates have decreased before the galaxies enter the main clusters (Goto et



al. 2003b; Goto et al. 2003c). In Paper I, we argued that the ‘pre-processing’ occurred in the subclusters (Zabludoff, Mulchaey 1998; Hashimoto, Oemler 2000; Balogh et al. 2000), which is consistent with the observations showing that red galaxies have a clumpy distribution around a main-cluster (Kodama et al. 2001). In the subclusters of the LCL at  $z \sim 0.5$ , ram-pressure stripping is marginally effective ( $0.2 \lesssim r_{\text{st}}/r_{\text{vir}} \lesssim 0.3$ ) in the non-heated ICM, and it is ineffective in the heated ICM model (figures 3 and 4). If ram-pressure stripping is the mechanism of the pre-processing, most of the cold gas in galaxies may be removed and star-formation activity of the galaxies may completely die out before the galaxies enter the main cluster. This may be inconsistent with the existence of many blue galaxies in main clusters at  $z \lesssim 0.5$  (Kodama, Bower 2001); the observations suggest a slower decline of the star-formation rates. Thus, the heated ICM model is preferable because ram-pressure stripping can be ignored. In the heated ICM model, evaporation can be candidates of the mechanism of the pre-processing. The time-scale of the evaporation is  $0.5 \lesssim t_{\text{evap}} \lesssim 10$  Gyr. Since the time-scale is relatively large, the evaporation can be an alternative of strangulation, which is expected to gradually suppress the star-formation activities of galaxies (Larson et al. 1980; Kodama et al. 2001; Bekki et al. 2002), but is highly speculative (Benson et al. 2000).

For the HCL observed at  $z \sim 1$ , ram-pressure stripping is effective in the main cluster regardless of non-gravitational heating. As is the case of the LCL at  $z \sim 0.5$ , the ICM of the subclusters must have been heated to avoid ram-pressure stripping in the subclusters.

At higher redshifts ( $z \gtrsim 1$ ), the effect of the disk evolution is more significant (figures 3 and 4), although it is not well-known that disk galaxies with the rotation velocities that we studied exist. At these redshifts, most of the subclusters have not been absorbed in the main cluster. As long as the ICM has not been heated non-gravitationally, the efficiency of ram-pressure stripping decreases only slowly as redshift increases. Thus, the products of ram-pressure stripping, such as galaxies that have spectra reflecting rapidly declined star-formation rates, may be observed at these redshifts although the number fraction is not as much as that at lower redshifts. In the non-heated ICM model, figure 7 shows that the evaporation is ineffective ( $t_{\text{cond}} \gtrsim t_{\text{H}}$ ) for less massive systems such as the subclusters of the LCL (at  $z > 0.7$ ) and the HCL (at  $z > 1.5$ ). Thus, if the evaporation is the mechanism of the pre-processing, the star-formation rates of galaxies hardly decline in the vicinity of the clusters at  $z \gtrsim 1$ –2 except for galaxies in which star-formation activities decrease rapidly by the ram-pressure stripping. On the other hand, if the ICM has been heated, ram-pressure stripping does not occur in the high-redshift range (figures 3 and 4). The time-scale of the evaporation is given by  $t_{\text{cond}}(r=0) \lesssim t_{\text{evap}} \lesssim t_{\text{cond}}(r_{\text{vir}})$  and is relatively large; for example,  $1 \lesssim t_{\text{evap}} \lesssim 4$  Gyr at  $z \sim 2$  for the subcluster of the LCL (figure 6). Thus, the star-formation rates of galaxies should decrease slowly with this time-scale. Thus, the heated and non-heated ICM models may be discriminated by future observations of the star-formation history of galaxies in the regions surrounding main clusters. However, quantitative predictions based on semi-analytic models

or numerical simulations would be required for actual discrimination. We leave this for future study.

## 5. Conclusions

We have investigated ram-pressure stripping and evaporation of disk galaxies in and around a cluster using analytical models based on a hierarchical clustering scenario. We considered the redshift evolution of the size and surface density of the disk. We showed that the evolution does not much affect the efficiency of ram-pressure stripping of galaxies for  $z \lesssim 0.5$ , but affects for  $z \gtrsim 1$ . We also considered the saturation of thermal conduction in detail, and found that it cannot be ignored at larger radii of a cluster, which makes the time-scale of the evaporation larger. Thus, the evaporation has the same effect as strangulation (stripping of warm gas in galactic halos) to suppress the star-formation activities of galaxies gradually. Observations of galaxies in the vicinity of clusters at  $z \sim 1$  are useful to investigate whether non-gravitational heating has occurred or not by  $z \sim 1$ .

We are grateful to M. Nagashima and M. Enoki for useful comments. Y. F. was supported in part by a Grant-in-Aid from the Ministry of Education, Culture, Sports, Science and Technology (14740175).

## References

- Abadi, M. G., Moore, B., & Bower, R. G. 1999, MNRAS, 308, 947
- Abraham, R. G., et al. 1996, ApJ, 471, 694
- Babul, A., Balogh, M. L., Lewis, G. F., & Poole, G. B. 2002, MNRAS, 330, 329
- Balogh, M. L., Babul, A., & Patton, D. R. 1999a, MNRAS, 307, 463
- Balogh, M. L., Morris, S. L., Yee, H. K. C., Carlberg, R. G., & Ellingson, E. 1997, ApJ, 488, L75
- Balogh, M. L., Morris, S. L., Yee, H. K. C., Carlberg, R. G., & Ellingson, E. 1999b, ApJ, 527, 54
- Balogh, M. L., Navarro, J. F., & Morris, S. L. 2000, ApJ, 540, 113
- Balsara, D., Livio, M., & O’Dea, C. P. 1994, ApJ, 437, 83
- Bekki, K., Couch, W. J., & Shioya, Y. 2002, ApJ, 577, 651
- Benson, A. J., Bower, R. G., Frenk, C. S., & White, S. D. M. 2000, MNRAS, 314, 557
- Bond, J. R., Cole, S., Efstathiou, G., & Kaiser, N. 1991, ApJ, 379, 440
- Bower, R. G. 1991, MNRAS, 248, 332
- Butcher, H., & Oemler, A., Jr. 1978, ApJ, 219, 18
- Butcher, H., & Oemler, A., Jr. 1984, ApJ, 285, 426
- Byrd, G., & Valtonen, M. 1990, ApJ, 350, 89
- Couch, W. J., Barger, A. J., Smail, I., Ellis, R. S., & Sharples, R. M. 1998, ApJ, 497, 188
- Couch, W. J., & Sharples, R. M. 1987, MNRAS, 229, 423
- Cowie, L. L., & McKee, C. F. 1977, ApJ, 211, 135
- Cowie, L. L., & Songaila, A. 1977, Nature, 266, 501

- Dressler, A. 1980, ApJ, 236, 351
- Dressler, A., et al. 1997, ApJ, 490, 577
- Dressler, A., Oemler, A., Jr., Butcher, H. R., & Gunn, J. E. 1994, ApJ, 430, 107
- Ellingson, E., Lin, H., Yee, H. K. C., & Carlberg, R. G. 2001, ApJ, 547, 609
- Fasano, G., Poggianti, B. M., Couch, W. J., Bettoni, D., Kjærgaard, P., & Moles, M. 2000, ApJ, 542, 673
- Fujita, Y. 1998, ApJ, 509, 587
- Fujita, Y. 2001a, ApJ, 550, 612
- Fujita, Y. 2001b, ApJ, 550, L7
- Fujita, Y. 2004, PASJ, 56, 29 (Paper I)
- Fujita, Y., & Nagashima, M. 1999, ApJ, 516, 619
- Fujita, Y., Sarazin, C. L., Nagashima, M., & Yano, T. 2002, ApJ, 577, 11
- Fujita, Y., & Takahara, F. 2000, ApJ, 536, 523
- Fujita, Y., Takizawa, M., Nagashima, M., & Enoki, M. 1999, PASJ, 51, L1
- Gaetz, T. J., Salpeter, E. E., & Shaviv, G. 1987, ApJ, 316, 530
- Goto, T., et al. 2003a, PASJ, 55, 739
- Goto, T., et al. 2003b, PASJ, 55, 757
- Goto, T., Yagi, M., Tanaka, M., & Okamura, S. 2004, MNRAS, 348, 515
- Goto, T., Yamauchi, C., Fujita, Y., Okamura, S., Sekiguchi, M., Smail, I., Bernardi, M., & Gomez, P. L. 2003c, MNRAS, 346, 601
- Gunn, J. E., & Gott, J. R., III 1972, ApJ, 176, 1
- Hashimoto, Y., & Oemler, A., Jr. 2000, ApJ, 530, 652
- Kodama, T., & Bower, R. G. 2001, MNRAS, 321, 18
- Kodama, T., Smail, I., Nakata, F., Okamura, S., & Bower, R. G. 2001, ApJ, 562, L9
- Lacey, C., & Cole, S. 1993, MNRAS, 262, 627
- Larson, R. B., Tinsley, B. M., & Caldwell, C. N. 1980, ApJ, 237, 692
- Lloyd-Davies, E. J., Ponman, T. J., & Cannon, D. B. 2000, MNRAS, 315, 689
- Loewenstein, M. 2000, ApJ, 532, 17
- Lubin, L. M. 1996, AJ, 112, 23
- Margoniner, V. E., & de Carvalho, R. R. 2000, AJ, 119, 1562
- Mo, H. J., Mao, S., & White, S. D. M. 1998, MNRAS, 295, 319
- Moore, B., Katz, N., Lake, G., Dressler, A., & Oemler, A., Jr. 1996, Nature, 379, 613
- Mori, M., & Burkert, A. 2000, ApJ, 538, 559
- Mulchaey, J. S. 2000, ARA&A, 38, 289
- Mulchaey, J. S., Davis, D. S., Mushotzky, R. F., & Burstein, D. 2003, ApJS, 145, 39
- Oemler, A., Jr., Dressler, A., & Butcher, H. R. 1997, ApJ, 474, 561
- Ponman, T. J., Cannon, D. B., & Navarro, J. F. 1999, Nature, 397, 135
- Portnoy, D., Pistinner, S., & Shaviv, G. 1993, ApJS, 86, 95
- Quilis, V., Moore, B., & Bower, R. 2000, Science, 288, 1617
- Rakos, K. D., Odell, A. P., & Schombert, J. M. 1997, ApJ, 490, 194
- Rakos, K. D., & Schombert, J. M. 1995, ApJ, 439, 47

- Schindler, S. 1999, A&A, 349, 435
- Smail, I., Edge, A. C., Ellis, R. S., & Blandford, R. D. 1998, MNRAS, 293, 124
- Takeda, H., Nulsen, P. E. J., & Fabian, A. C. 1984, MNRAS, 208, 261
- Toomre, A., & Toomre, J. 1972, ApJ, 178, 623
- Tormen, G., Moscardini, L., & Yoshida, N. 2004, MNRAS, 350, 1397
- van Dokkum, P. G., Franx, M., Kelson, D. D., Illingworth, G. D., Fisher, D., & Fabricant, D. 1998, ApJ, 500, 714
- Voit, G. M., Bryan, G. L., Balogh, M. L., & Bower, R. G. 2002, ApJ, 576, 601
- Whitmore, B. C., & Gilmore, D. M. 1991, ApJ, 367, 64
- Whitmore, B. C., Gilmore, D. M., & Jones, C. 1993, ApJ, 407, 489
- Yamada, M., & Fujita, Y. 2001, ApJ, 553, L145
- Zabludoff, A. I., & Mulchaey, J. S. 1998, ApJ, 496, 39